Electronic Supplementary Information

Two-dimensional fingerprint nanoprobe based on black phosphorus for bio-SERS analysis and chemo-photothermal therapy

Zhiming Liu,‡*[a] Haolin Chen,‡[b] Yali Jia,[c] Wen Zhang,[d] Henan Zhao,[a] Wendong Fan,[e] Wolun Zhang,[a] Huiqing Zhong,[a] Yirong Ni[a] and Zhouyi Guo*[a]

a. MOE Key Laboratory of Laser Life Science & SATCM Third Grade Laboratory of Chinese Medicine and Photonics Technology, College of Biophotonics, South China Normal University, Guangzhou, Guangdong 510631, P. R. China

b. Key Laboratory of Sensing Technology and Biomedical Instrument of Guangdong Province, School of Biomedical Engineering, Sun Yat-sen University, Guangzhou, Guangdong 510006, P. R. China

c. Casey Eye Institute, Oregon Health & Science University, 3375 S.W. Terwilliger Blvd., Portland, OR 97239-4197, USA

d. Institute for Brain Research and Rehabilitation, South China Normal University, Guangzhou, Guangdong 510631, P. R. China

e. NHC Key Laboratory of Assisted Circulation (Sun Yat-sen University), Guangzhou 510080, China

‡These authors contributed equally to the work.

*Corresponding authors: liuzm021@126.com (Z. Liu); ann@scnu.edu.cn (Z. Guo)

Experimental Section

Materials

The bulk BP crystals were obtained from a commercial supplier (XFNANO, Nanjing, China) and stored in a dark Ar-filled glovebox. Chloroauric acid ($HAuCl_4 \cdot 4H_2O$) and N-methyl-2-pyrrolidone (NMP) were purchased from China National Medicine Corporation (Shanghai, China). Chlorpromazine, amiloride, methyl-β-cyclodextrin, sodium azide, hoechst 33258 and poly(ethylene glycol) methyl ether thiol (mPEG-SH, MW=5000) were obtained from Sigma-Aldrich. Doxorubicin hydrochloride, dimethyl sulfoxide, MTT, and rhodamine B (Rho B) were provided by Aladdin (Shanghai, China). Dulbecco's modified Eagle's medium (DMEM), Roswell Park Memorial Institute (RPMI)-1640, fetal bovine serum (FBS), penicillin and streptomycin were obtained from GIBCO (Grand Island, NY, United States). Other reagents were of analytical grade and were used as received without further purification. Deionized water (Milli-Q System, Millipore, USA) was used in all experiments.

Synthesis of BP-Au Nanohybrids

The BP nanosheets were prepared by liquid exfoliation of bulk crystals according to the literature with some modification.[1] In detail, 30 mg of the BP powder was added to a 50 mL sealed plastic pipe containing 30 mL of NMP. The mixture was sonicated with an ultrasonic probe at 600 W for 6 h followed by an ultrasonic bath (300 W, 25 ^oC) for 10 h. The precipitate was collected by centrifugation at 7000 rpm for 20 min and re-suspended in NMP. To remove the oversized particles, the resulting dispersion was centrifuged for 10 min at 1500 rpm. For nanocomposites synthesis, 50 µL of BP (5 $mg\ mL^{-1}$) was added to 20 mL of boiling H_2O with constant stirring. Meanwhile, 150 µL of $HAuCl_4$ aqueous solution (10 mM) was added into the solution and stirred for another 2 min. The color of the reaction mixture changed from pale yellow to red, indicating the formation of Au nanostructures. The resulting product was acquired after three times of centrifugation (5000 rpm, 15 min) and was redispersed in deionized water for further use. Citrate-stabilized AuNPs was synthesized according to the classical procedure using sodium citrate as the reductant.

Characterization

Transmission electron microscopic (TEM) analysis was carried out using a FEI Tecnai G2 Spirit T12 (Hillsboro, Oregon, USA) operated at 120 kV equipped with an energy-dispersive x-ray (EDX) spectrometer. High-angle annular dark field scanning transmission electron microscopy (HAADF-STEM) image of BP-AuNPs and corresponding elemental mapping images were performed using a FEI F30 transmission electron microscope at 300 kV. Ultraviolet-visible-near infrared

(UV-vis-NIR) absorbance spectra were obtained using a UV-vis-NIR spectrometer (UV-6100, MAPADA, China). Raman spectra were recorded using a Renishaw inVia microspectrometer (Derbyshire, England) equipped with the excitation wavelengths of 514.5 nm and 785 nm generated using an Ar^+ laser and a semiconductor laser, respectively. The XRD patterns were recorded on a Bruker D8 Advance (Bruker AXS, Germany) X-ray diffractometer with Cu Kα radiation (λ = 1.5406 Å). The zeta potentials of nanomaterials were measured on Malvern Zetasizer Nano ZS analyzer.

SERS Experiments

4T1, Hela and Hep G2 cells, obtained from the Laboratory Animal Center of Sun Yat-sen University (Guangzhou, China), were pre-cultured in RPMI-1640 or DMEM medium supplemented with 10% FBS, penicillin (100 units mL^{-1}), and streptomycin (100 mg mL^{-1}) in 5% CO2 and 95% air at 37 °C in a humidified incubator. Then the cells were seeded onto sterile quartz coverslips in cell culture petri dishes (35 mm) with 2 mL of medium for 24 h to reach 70-80% confluence. Subsequently, medium containing BP-AuNPs or AuNPs at a concentration of 32 μg mL^{-1} was added for several hours incubation. After that, the living cells were rinsed five times with PBS and re-incubated in PBS for SERS detection. Raman spectroscopic measurements were conducted using the Renishaw inVia confocal Raman system (controlled by WiRE 3.4 software) equipped with a 785 nm NIR semiconductor laser and coupled to a Leica DM-2500M microscope. A 50× objective lens (NA 0.75, ~1 μm laser spot size) was chosen for cellular detection. The NIR laser power on the sample was below 10 mW to avoid laser-induced heating. The Raman spectra were recorded in static mode for a 2 s laser exposure over a wavenumber range of 600-1720 cm^{-1}. Fluorescence background subtraction from the raw data and spectra smoothing were performed before further analysis. For PCA-LDA, mean SERS spectrum was acquired by averaging the Raman data of more than 50 cells per group (10 spectral lines per cell). The data were then analyzed using PCA-LDA in the Matlab software (The Mathworks, Inc., Natick, MA). Raman spectral mapping was performed in the Streamline mode at 1.2 s exposure time with a wavenumber center at 1200 cm^{-1}. For ultrafast NIR SERS imaging, the integration time was 0.19 s (35 ms per pixel). Label-free SERS images were acquired using the integrated signal-to-baseline intensities from 620 to 1720 cm^{-1}. BP-Au nanohybrids mediated photothermolysis was performed at the interval of two rounds of Raman scanning. Hep G2 cells containing 32 μg mL^{-1} of BP-AuNPs grown on the sterile quartz coverslips and were placed under the microspectrometer. A high power of NIR laser (785 nm, 100 mW) with a long irradiation time (~10 min) was used to allow the photothermal ablation of cancer cells. The SERS images and spectral lines of Hep G2 cells were obtained before and after the photothermal ablation experiment. To investigate the endocytosis mechanism of BP-AuNPs, BP-AuNPs/Rho B was firstly prepared by mixing the solution of BP-AuNPs and Rho B (20 mg) with constant stirring overnight in a dark room followed by three times of centrifugation (7000 rpm,

10min), then the Hep G2 cells, pre-treated with amiloride (80 μg mL^{-1}), chlorpromazine (15 μg mL^{-1}), MβCD (8 mM) or NaN_3 (40 mM) for 2 h, were incubated with BP-AuNPs/Rho B for 6 h, then the cells were observed under a fluorescence microscope.

Hemolysis assay

Human blood obtained from healthy volunteers was centrifuged at 3000 rpm for 5 min (4 °C) and washed several times with PBS solution to obtain pure erythrocytes. Then, 4% erythrocytes (v/v) was mixed with the same volume of water (positive control), PBS (negative control) or BP-AuNPs solution at various concentrations. The mixture was incubated at 37 °C for 2 h. After centrifugation, the supernatants were collected, and the absorbance at 541 nm was recorded using a UV-vis spectrophotometer. The percentage of hemolysis was calculated using the following equation:

$$\text{Hemolysis } (\%) = \frac{(A_{sample} - A_{negative\ control})}{(A_{positive\ control} - A_{negative\ control})} \times 100\% \quad (1)$$

Preparation of BAPD and its drug-delivery feature

Before drug loading, PEGylated BP-AuNPs (BAP) were synthesized by mixing BP-AuNPs (0.1 mg mL^{-1}, 10 mL) with the same mass of mPEG-SH, and the products were purified by centrifugation at 5000 rpm for 10 min. To load DOX onto BAP, different concentrations of DOX (0.05, 0.1, 0.15, 0.20, 0.25 and 0.30 mg mL^{-1}) were mixed with BAP (100 μg mL^{-1}) to achieve different mass ratio. After overnight stirring, unbound DOX was removed by centrifugation. The resulting BAPD was resuspended and stored at 4 °C. To evaluate the DOX-loading efficiency, the content of DOX in the supernatant was measured by absorbance spectrometer. The drug loading efficiency (DLE) was calculated by the following equation:

$$\text{DLE}\% = \left(\frac{W_{initial\ DOX} - W_{DOX\ in\ supernatant}}{W_{initial\ DOX}}\right) \times 100\% \quad (2)$$

where $W_{initial\ DOX}$ and $W_{DOX\ in\ supernatant}$ were the weights of DOX in original and residual DOX solution, respectively. To study the release behavior of DOX, the BAPD suspension was added into dialysis bag and dialyzed in PBS at pH 7.4 and 5.5, respectively. The laser-induced drug release behavior was studied in a similar procedure. At predetermined time intervals, the sample was irradiated with a NIR laser (808 nm, 2 W cm^{-2}) for 5 min.

Photothermal Effect of BAP

The nanostructure suspensions were diluted to different concentrations, and then irradiated with the 808 nm laser with a power density of 2 W cm^{-2} for 10 min. The temperatures of the solutions were measured every 30 s using a thermocouple thermometer or an infrared thermal camera (Fluke Ti200, Fluke Corp, USA). To evaluate the

photothermal stability, the BAP solution was exposed to 808 nm laser for 10 min (laser on), followed by naturally decreased to room temperature after the NIR laser was turned off (laser off); this procedure was repeated five times.

The photothermal conversion efficiency (η) is calculated using the following Eqs.[1]:

$$\eta = \frac{hS(T_{max}-T_{surr})-Q_{dis}}{I\left(1-10^{-A_{808}}\right)} \quad (3)$$

$$\tau_S = \frac{m_D C_D}{hS} \quad (4)$$

where *h* is the heat transfer coefficient, *S* is the surface area of the container, *I* expresses the NIR laser power (808 nm, 2 W cm^{-2}), A_{808} means the absorbance at 808 nm of the nanostructures (OD_{BP}=0.49, OD_{BAP}=0.53), the equilibrium temperature is T_{max}, the ambient temperature of the surroundings is T_{surr}, and the heat associated with the light absorbance by the solvent is Q_{dis}. τ_s represents the sample system time constant, m_D and C_D mean the mass (1.2 g was used) and heat capacity (4.2 J g^{-1}), when pure water is used as the solvent. Pure water in a test tube was applied to measure the Q_{dis}.

***In vitro* experiments**

To assess the cytotoxicity of nanostructures, Hep G2, 4T1 and Hela cells pre-cultured in 96-well plates were incubated in DMEM or RPMI-1640 culture medium containing different concentrations of BAP for 24 h. Then the cell viabilities were measured by the standard MTT assay. For in vitro cancer therapy, Hep G2 cells were divided into seven groups: Control, Laser, BAP, BAPL, DOX, BAPD and BAPDL. After the cells were attached, the culture medium was replaced with medium containing various concentrations of free DOX, BAP or BAPD (with DOX loading capacity of 10% by weight) for further 6 h incubation. Then the cells were or were not irradiated by the NIR laser (808 nm, 2 W cm^{-2}) for 3 min and then incubated at 37 °C for a further 24 h. The anti-tumor effects of these treatments were assessed by the MTT assay. For fluorescence analysis, Hep G2 cells were seeded onto cell culture petri dishes (35 mm) overnight to 70-80% confluence. After that, the cells were exposed to DOX, BAP and BAPD at the DOX concentration of 4 μg mL^{-1}. Then the cells were irradiated with an 808 nm laser for 10 min and incubated at 37 °C for an additional 4 h. Before fluorescence imaging, the cells were fixed with 4% neutral buffered formalin for 10 min and then stained with Hoechst 33258 dye (4 μg mL^{-1}) for 10 min in the dark. After washing three times with PBS, the fluorescnet images were taken with the fluorescence microscope.

***In vivo* experiments**

Female Balb/c mice (4-5 weeks old) were purchased from Laboratory Animal Center of Sun Yat-Sen University, and performed with protocols approved by South China Normal University Animal Care and Use Committee.

4T1 cells (1×10^7) suspended in 100 μL of PBS were implanted into the dorsal subcutis of female Balb/c mice. When the tumor volume reached about 200 mm^3, the mice were used for experiment. First, the in vivo distribution of nanomaterials was study. NIR fluorescent (NIRF) dye-grafted nanocarrier was prepared by mixing BAP with Cyanine7 (Cy7) amine with constant stirring overnight in a dark room followed by centrifugation (7000 rpm, 10min). Then, BAP/Cy7 was intravenously injected into the tumor-bearing mice. The NIRF imaging was acquired using an IVIS Lumina III imaging system at different time points. For chemo-photothermal therapy, the mice were randomly divided into 5 groups (n=5 per group): PBS, BAP, DOX, BAPL and BAPDL. Hair was removed by clipping with an electric clipper 24 h prior to drug injection. After that, the mice were then intravenously injected with 100 μL of PBS, BAP, DOX and BAPD at the DOX concentration of 1 mg kg^{-1}, respectively. For NIR laser treated groups, the tumors were exposed to the NIR laser (808 nm, 2 W cm^{-2}) for 2.5 min after 24 h injection. The surface temperature of the tumor was monitored by the infrared thermal camera. The tumor volume was measured using a digital caliper every two days and calculated according to the following formula: $(\text{tumor width})^2 \times (\text{tumor length})/2$. Relative tumor volume was calculated as V/V_0, where V_0 was the tumor volume at initiation of the treatment. To assess the *in vivo* toxicity, the body weight of mice after treatment was measured every other day. At the end of experiment, all mice were sacrificed and the tumor tissues and major organs (heart, liver, spleen, lungs and kidney) were collected. For histological examination, the tissues from different groups were fixed in 4% formalin and processed routinely into paraffin for H&E staining using standard techniques. The slices were examined under the microscope.

Supplementary Tables

Table S1. The assignments of the Raman bands of Hep G2 cells incubated with AuNPs for 12 h.

Raman Shift (cm^{-1}) Hep G2	Tentative assignment [3-9]
833w	Tyr ring breath (p); O-P-O asym str (d)
1000w	Phe ring sym breath (p)
1029w	C-H in-plane Phe (p)
1129w	C-N str (p); Chain C-C str (l); Disaccharide: C-O/C-C (c)
1304w	Ring str, CH_2/CH_3 twist (p); A (d)
1352w	CH_2/CH_3 twist, CH_2/CH_3 wag (p)
1582w	amide II, Phe, Tyr (p); G, A (d)
2850-2960w	CH_2/CH_3 asym and sym str (p, l)

Abbreviations: p, protein; l, lipid; d, DNA/RNA; c, carbohydrate; Tyr, tyrosine; Cys, Cystine; Trp, Tryptophan; Phe, phenylalanine; A, adenine; T, thymine; C, cytosine; G, guanine; bend, bending; str, stretching; def, deformation; rocking; twist, twisting; breath, breathing; wag, wagging; sym, symmetrical; asym, asymmetrical; bk, backbone; s, strong; m, middle; w, weak.

Table S2. The assignments of the Raman bands of three kinds of tumor cells incubated with BP-AuNPs.

Raman Shift (cm^{-1})			Tentative assignment [3-9]
Hela	4T1	Hep G2	
636m	646m	638w	Tyr, COO- bend or C-S str (p)
656m		658m	C-C twist Tyr (p)
676w	677m	680w	C-S str Cys (p); G (d)
698w	696w	700w	Cholesterol (l)
731w	732w		A (d)
746w	749w	750m	T (d); Trp ring breath (p)
801m	805m		O-P-O str (d)

836s	835s	837s	Tyr ring breath (p); O-P-O asym str (d)
883w	879m	883w	Disaccharide: C-O-C skeletal mode (c)
931w	931w	931w	C-C bk str α helix (p); C-O-C glycos (c)
961m	962w	967m	C-C str (p)
		977s	Trp, Tyr ring def (p)
1001s	1005s	1001s	Phe ring sym breath (p)
1015s			DNA bk: C-O str (d)
1031s	1024s	1030s	C-H in-plane Phe (p)
1066m	1061w	1066w	C-N str (p); Chain C-C str (l)
1099w	1098m	1099m	O-P-O str (d); Chain C-C str (l); C-O str, C-C str (c)
1131s	1121s, 1131s	1124s, 1132s	C-N str (p); Chain C-C str (l); Disaccharide: C-O/C-C (c)
1160m	1168m		C-C/C-N str (p)
		1181w	Tyr ring def (p)
1214m	1208w		Phe C-C_6H_5 str, Trp (p)
	1231w	1226w	Amide III random coils (p)
1254w	1254w	1265m	Amide III β sheet (p), CH_2/CH_3 def (p, l)
1276m	1276m		Amide III α helix (p), CH_2/CH_3 def (p, l)
	1308s	1297s	CH_2 def (l); A, C (d)
1316s		1316s	Ring str, CH_2/CH_3 twist (p); A (d)
1351s	1339s, 1356s	1355s	CH_2/CH_3 twist, CH_2/CH_3 wag (p)
		1396m	COO- sym str (p)
1418m	1422m	1418m	CH_3 asym str (p, l)
1456m		1456w	CH_2 def (p)
1482w	1482m	1496w	G, A (d)
1514w	1519w		A, T (d)
1539w		1533 w	A, C, G (d)
1570m	1549w, 1561m	1558m	Amide II, Trp (p)
1585s	1579s	1586m	Amide II, Phe, Tyr (p); G, A (d)
1595s			COO- sym str, Phe, Tyr (p); A (d)
1611m	1605s	1611m	Tyr, Phe C=C bend (p)
		1625m	C=C olefinic str (p, d, l)
1663w	1666w		Amide I: α helix (p)
2850-2960m	2850-2960m	2850-2960m	CH_2/CH_3 asym and sym str (p, l)

Abbreviations: p, protein; l, lipid; d, DNA/RNA; c, carbohydrate; Tyr, tyrosine; Cys, Cystine; Trp, Tryptophan; Phe, phenylalanine; A, adenine; T, thymine; C, cytosine; G, guanine; bend, bending; str, stretching; def, deformation; rocking; twist, twisting; breath, breathing; wag, wagging; sym, symmetrical; asym, asymmetrical; bk, backbone; s, strong; m, middle; w, weak.

Table S3. Cell classification results based on leave-one-out cross-validation method.

Cell type	Raman prediction			Total
	4T1	Hela	Hep G2	
4T1	46	6	7	**59**
Hela	3	37	20	**60**
Hep G2	1	10	69	**80**
Sensitivity (%)	78.0%	61.7%	86.3%	
Specificity (%)	97.1%	66.2%	58.8%	

Table S4. The assignments of some SERS bands of Hep G2 cells before and after photothermal ablation.

Raman Shift (cm^{-1})		Tentative assignment [3-9]
Before	**After**	
638	644 ↑	Tyr, COO- bend, C-S str (p)
680	687 ↑	C-S str Cys (p); G (d)
750		T (d); Trp ring breath (p)
815	815 ↑	Phosphate: O-P-O str (d)
837	839 ↑	Tyr ring breath (p); O-P-O asym str (d)
	860	Ribose: C-C str, ring breath, C-O-C str (d)
883	891 ↑	Disaccharide: C-O-C skeletal mode (c)
931	931 ↑	α helix C-C bk str (p); C-O-C glycos (c)
	954	C-C bk str (p)
977	979 ↑	Trp, Tyr ring def (p)
1001	1001 ↑	Phe ring sym breath (p)
1015	1015 ↑	DNA bkb: C-O str (d)
1030	1030 ↑	C-H in-plane Phe (p)
1066	1070 ↓	C-N str (p); Chain C-C str (l)
1132	1132 ↑	C-N str (p); Chain C-C str (l); Disaccharide: C-O/C-C (c)

	1168	C-C/C-N str (p)
1226	1231 ↑	Amide III random coils (p)
1296	1288 ↑	Amide III α helix (p); A, C (d)
	1306	CH_2 def (l); A, C (d)
1316	1326 ↑	Ring str, CH_2/CH_3 twist (p); A (d)
1355	1352 ↑	CH_2/CH_3 twist, CH_2/CH_3 wag (p)
	1376	T, G, A (d)
1396	1396 ↓	COO- sym str (p)
1418		CH_3 asym str (p, l)
1456	1460 ↑	CH_2 def (p)
1482		G, A (d)
1533	1508	G, A, C (d)
1586	1574 ↑	Amide II, Phe, Tyr (p); G, A (d)
1605	1605 ↓	Tyr, Phe C=C bend (p)
1625		C=C olefinic str (p, d, l)

Abbreviations: p, protein; l, lipid; d, DNA/RNA; c, carbohydrate; Tyr, tyrosine; Cys, Cystine; Trp, Tryptophan; Phe, phenylalanine; A, adenine; T, thymine; C, cytosine; G, guanine; bend, bending; str, stretching; def, deformation; rocking; twist, twisting; breath, breathing; wag, wagging; sym, symmetrical; asym, asymmetrical; bk, backbone.

Table S5. The zeta potential of BP nanosheets after surface functionalization.

	BP	BP-AuNPs	BAP	BAPD
Zeta-potential (mV)	-28.3±0.86	-28.0±0.64	-30.1±1.70	22.1±1.25

Supplementary Figures

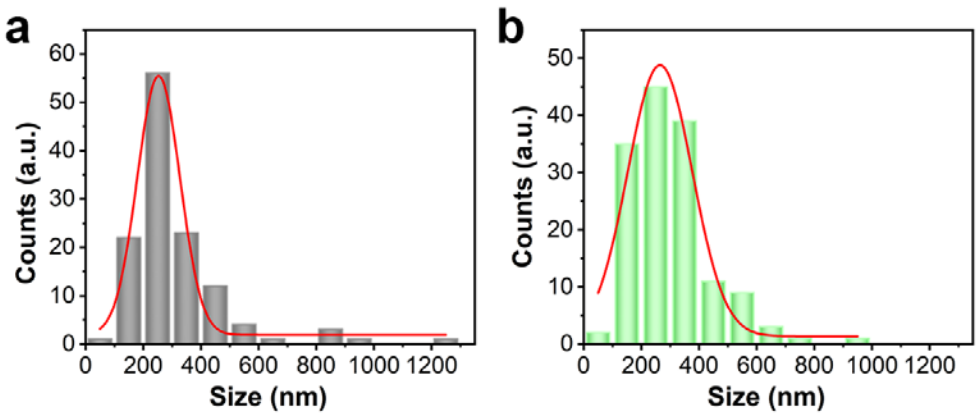

Fig. S1 Flake lateral length histograms of BP nanosheets (a) and BP-AuNPs (b), calculated from the TEM images.

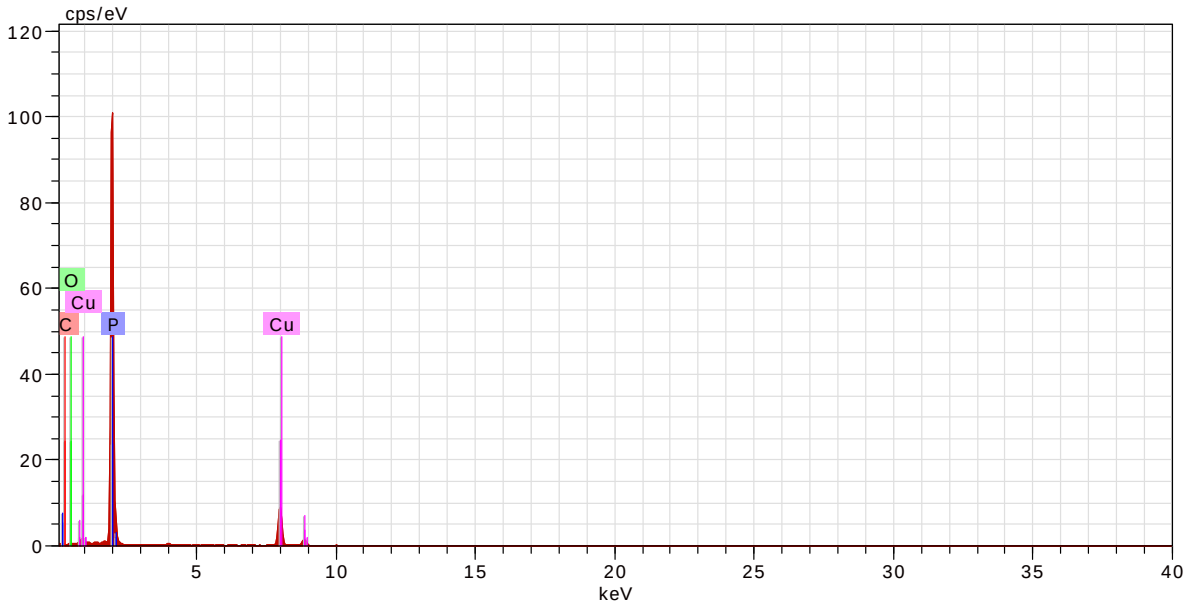

Fig. S2 EDX pattern of BP nanosheets.

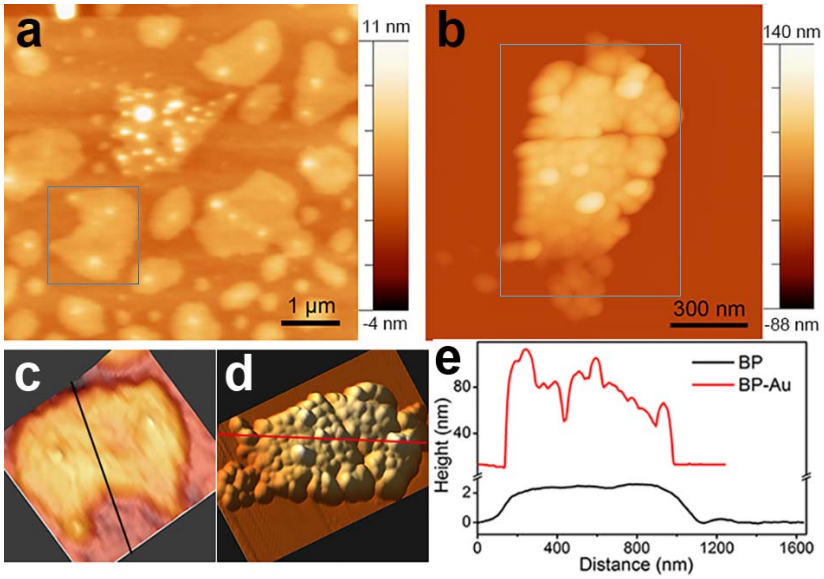

Fig. S3 AFM images (a, b) and corresponding 3D AFM topographies (c, d) of BP sheets and BP-AuNPs. (e) Height profiles along the lines in c and d. AFM images were recorded on a FM-Nanoview 1000 (FSM-Precision, China) using the tapping mode.

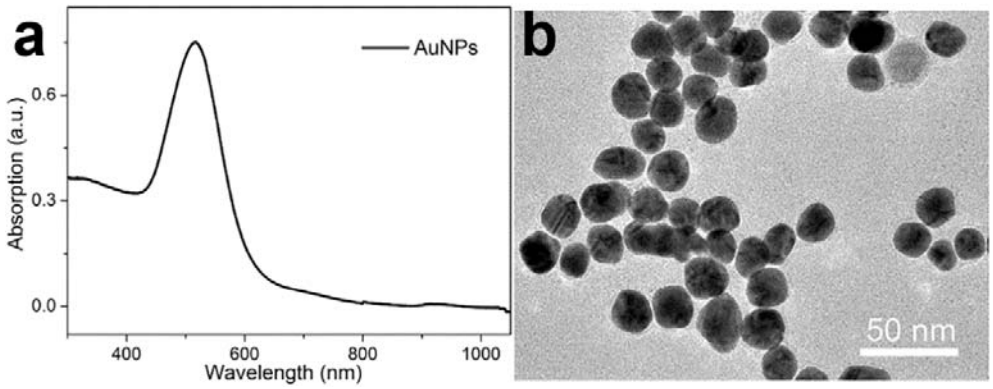

Fig. S4 Characterization of the citrate-stabilized AuNPs. (a) UV-vis-NIR absorbance spectrum; (b) TEM image.

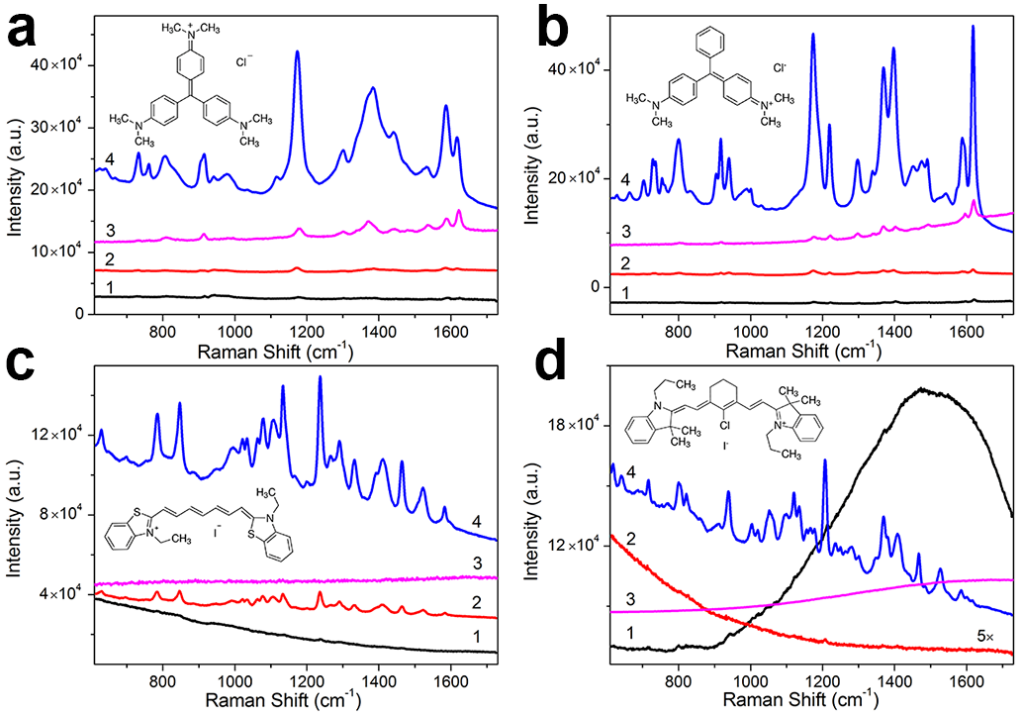

Fig. S5 SERS activity of BP-AuNPs. SERS experiments were carried out using crystal violet (CV) (a), malachite green (MG) (b), 3,3'-diethylthiatricarbocyanine iodide (DTTC) (c) and IR-780 (d) as the model Raman probes. The spectral lines represent the normal Raman spectra of the four dyes at the concentration of 10 mM under 785 nm excitation (1), the SERS spectra induced by citrate-stabilized AuNPs under 785 nm excitation (2), the SERS spectra induced by BP-AuNPs under 514.5 nm (3) and 785 nm (4) laser excitation, respectively. Experimental details: 10 µL of as-prepared BP-AuNPs (200 µM, elemental gold concentration) was mixed with 10 µL of different dyes (CV (10 µM), MG (10 µM), DTTC (1 µM) or IR-780 (1 µM)). Then the mixture was placed under the Renishaw inVia microspectrometer for SERS measurment. A 20× objective lens was used to focus the laser beam and to collect the Raman signal. The laser powers on samples were about 2 mW and 0.1-5 mW for visible and NIR lasers, respectively. The Raman spectra were recorded in the range of 600-1720 cm^{-1} during a 5 s acquisition.

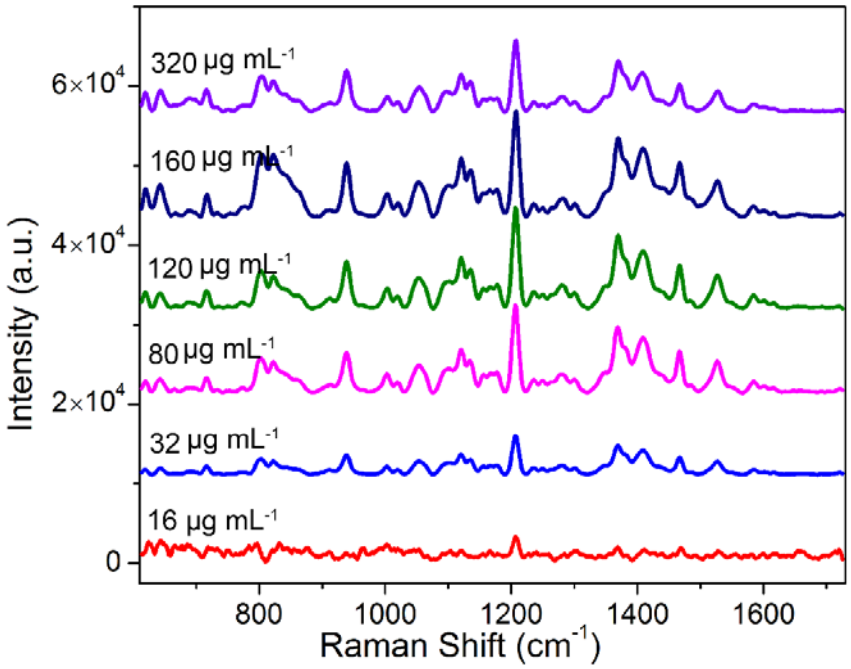

Fig. S6 The optimal concentration of BP-AuNPs for SERS detection using IR-780 as the Raman probe.

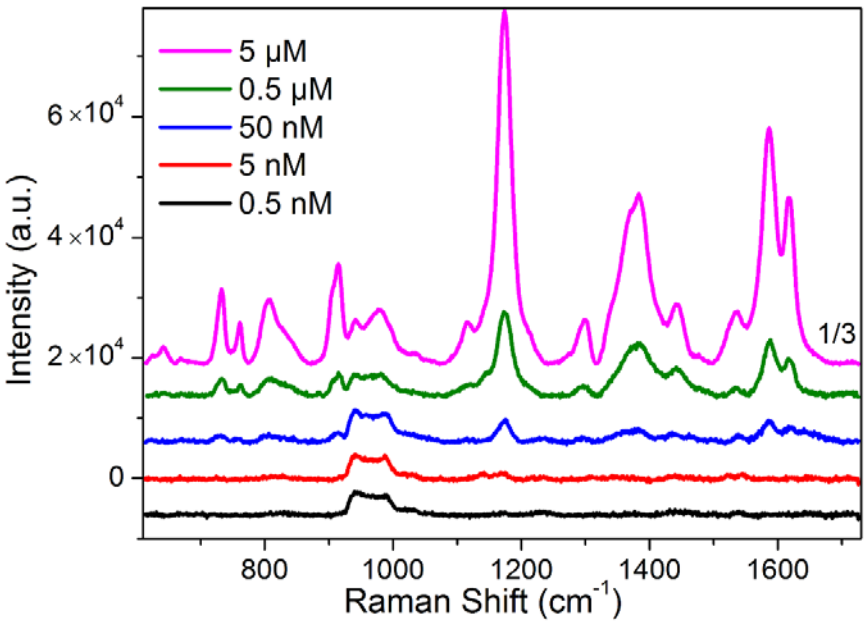

Fig. S7 SERS spectra of CV with different concentrations induced by BP-AuNPs with the concentration at 120 μg mL^{-1}.

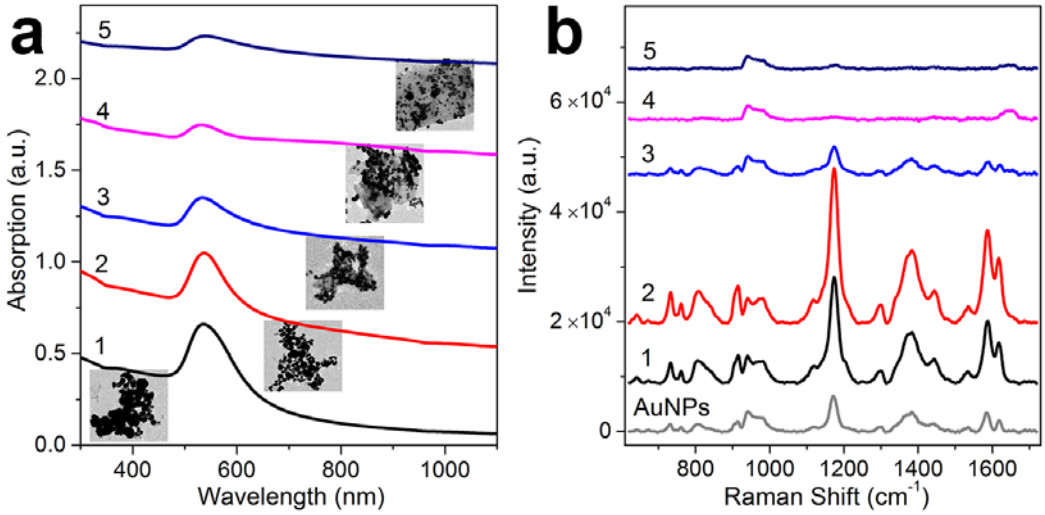

Fig. S8 Optimization of the BP-Au nanostructures. (a) UV-vis-NIR absorbance spectra and corresponding TEM images (inset) of BP-AuNPs prepared with different weight ratios between BP and chloroauric acid: (1) 2:5; (2) 4:5; (3) 8:5; (4) 12:5; (5) 18:5. (b) The SERS activities of the as-prepared BP-AuNPs using CV as the Raman probe.

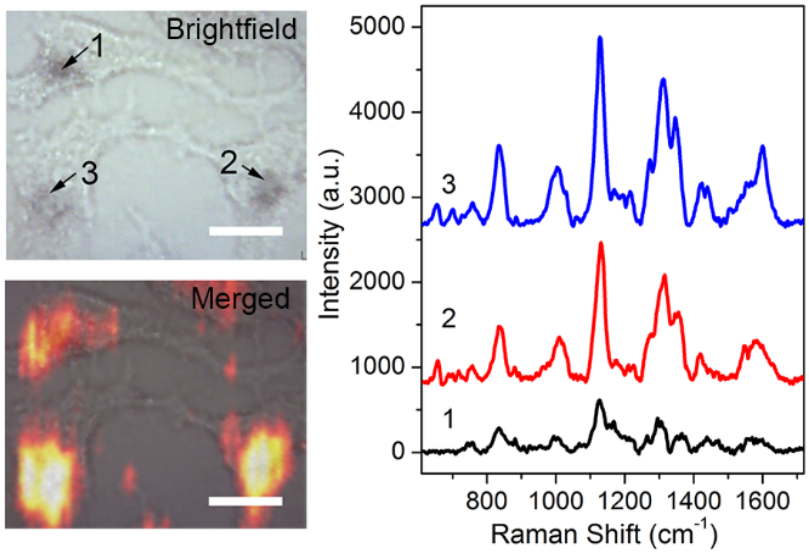

Fig. S9 NIR SERS imaging and spectra of Hep G2 cells containing BP-AuNPs with various degrees of aggregation. Scale bar: 20 μm.

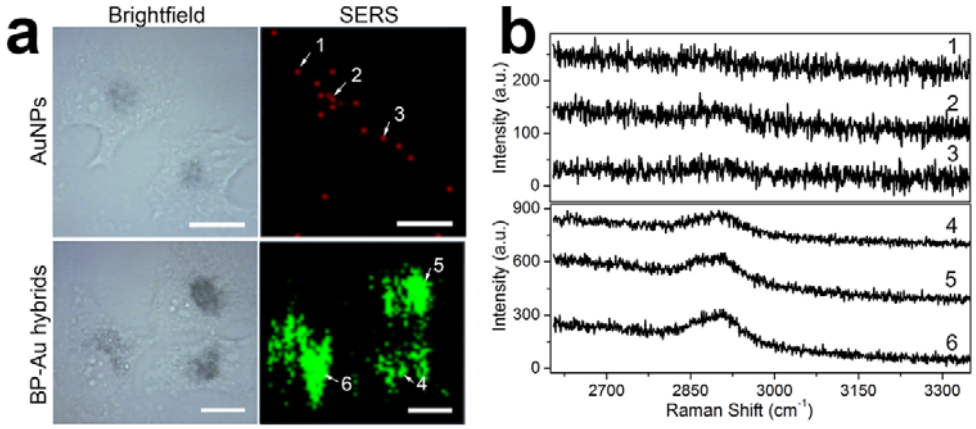

Fig. S10 (a) NIR SERS imaging of Hep G2 cells in the high-wavenumber region. (b) Tpyical SERS spectra acquired from the arrow-indicated regions. Scale bar: 20 μm.

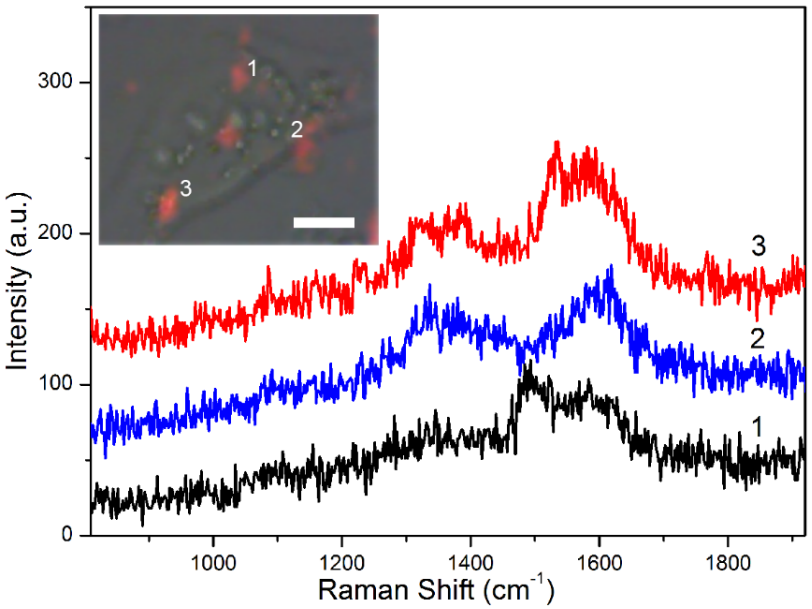

Fig. S11 SERS spectra of cancer cells incubated with GO-metal based SERS substrate, which is disturbed by the intrinsic Raman features of GO sheet (D and G bands: 1200-1700 cm^{-1}). Inset shows the overlap of brightfield and SERS images. Scale bar: 10 μm.

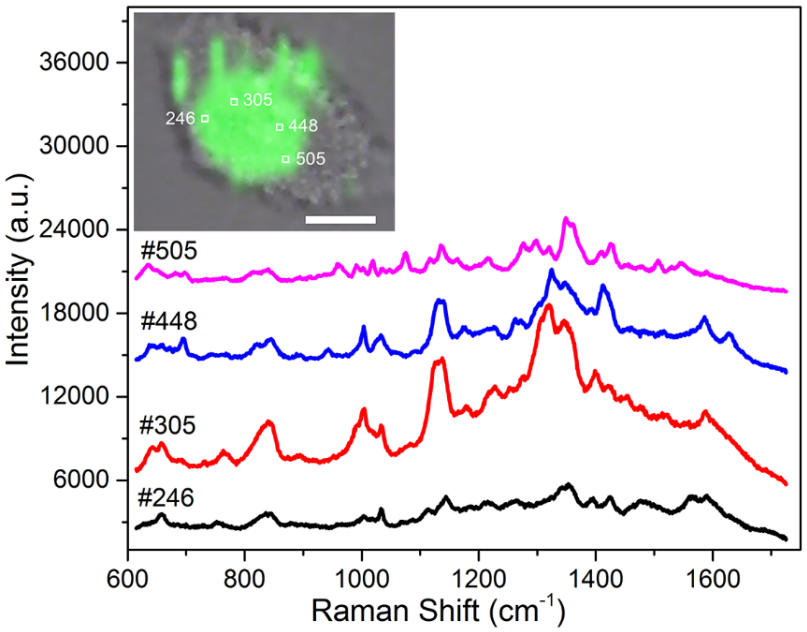

Fig. S12 Raw SERS spectra collected from four random pixel points in the Hep G2 cells incubated with BP-AuNPs, where no interference from the SERS substrate is observed. Inset shows the overlap of brightfield and SERS images. Scale bar: 10 µm.

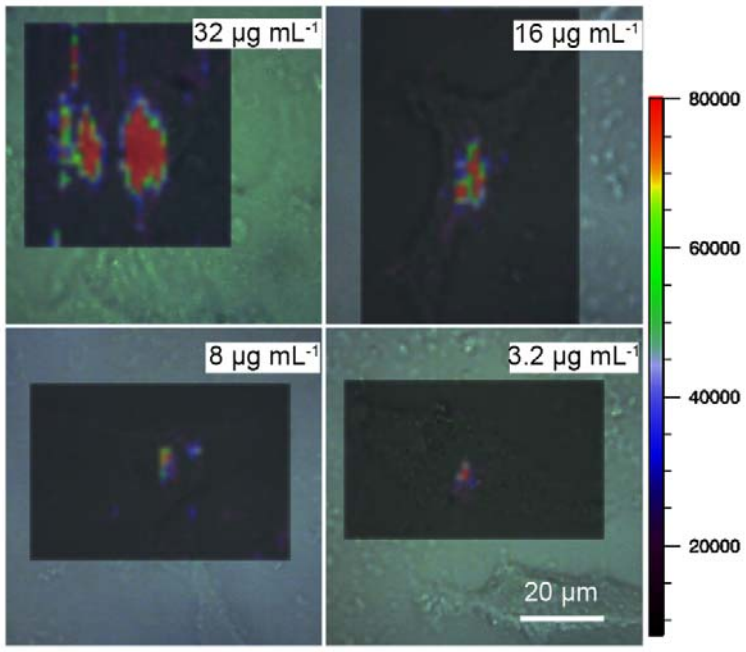

Fig. S13 NIR SERS images of Hep G2 cells incubated with various concentrations of BP-AuNPs.

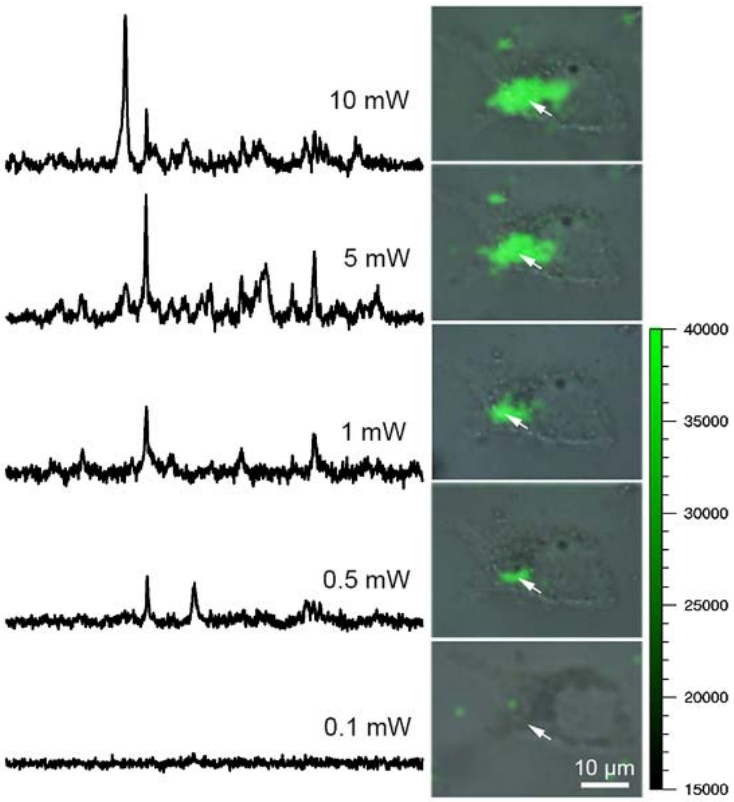

Fig. S14 NIR SERS images of a typical Hep G2 cell induced by BP-AuNPs under different power densities of 785 nm laser irradiation.

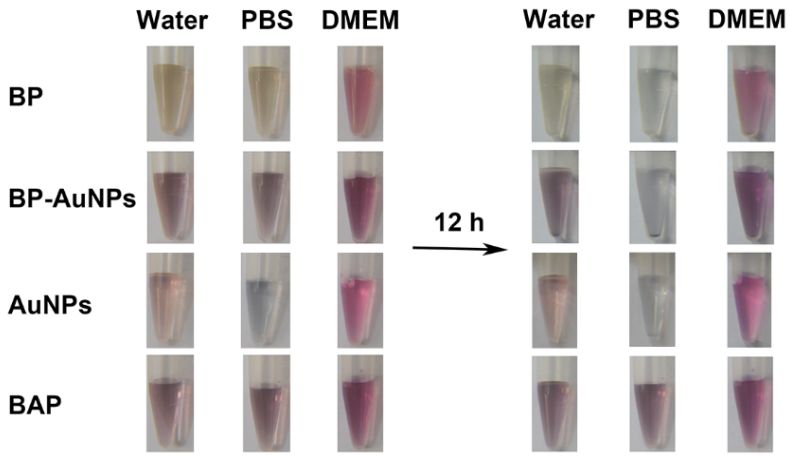

Fig. S15 The dispersion of nanostructures in different physiological environments.

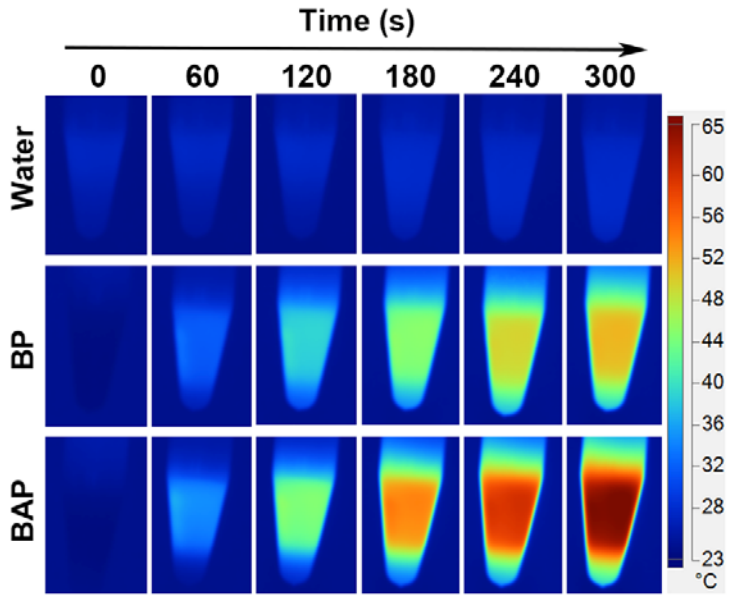

Fig. S16 Infrared thermal images of BP and BAP solutions (200 μg mL^{-1}) under 808 nm laser irradiation (2 W cm^{-2}).

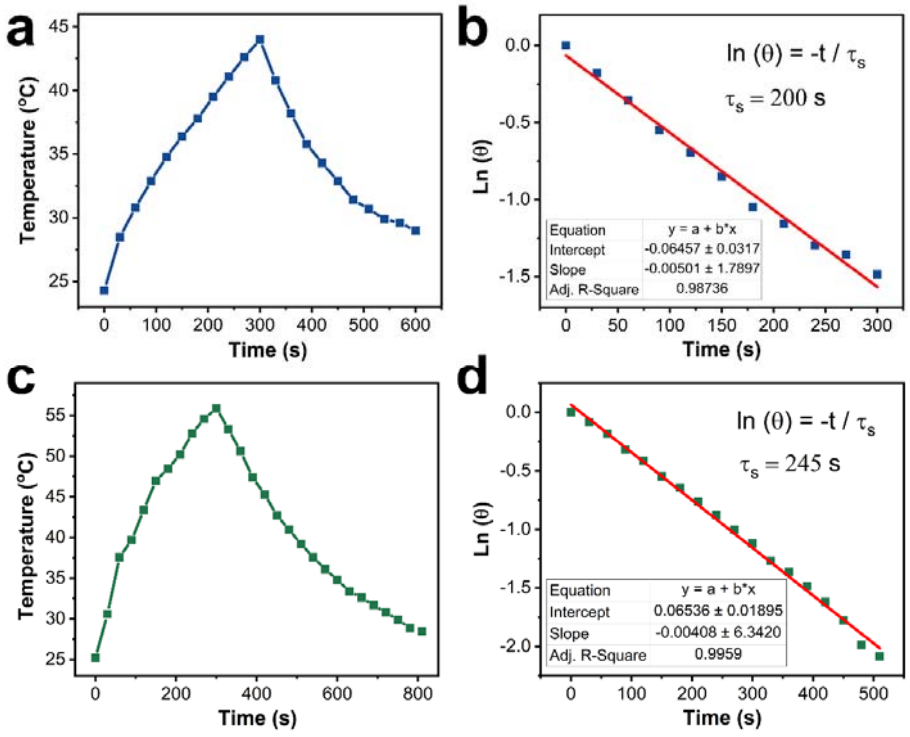

Fig. S17 Photothermal properties of BP NSs (a, b) and BAP (c, d). Plots of the temperature vs time for BP NSs (a) and BAP (c) during laser irradiation and cooling (laser off). b and d show the cooling time vs ln (θ). On the basis of the linear regression analysis, the τ_s values (the slope of the plot) for BP NSs and BAP are determined to be 200 s and 245 s, respectively. The η values for BP NSs and BAP are calculated to be 32.8% and 43.0%, respectively.

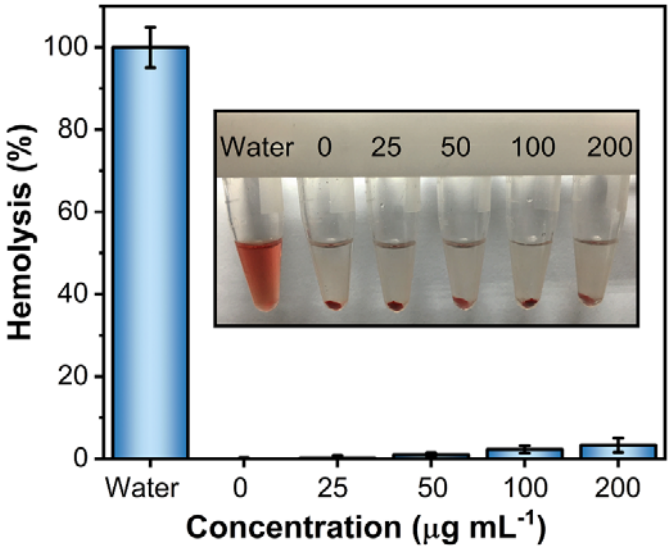

Fig. S18 The hemolysis assay of BP-AuNPs.

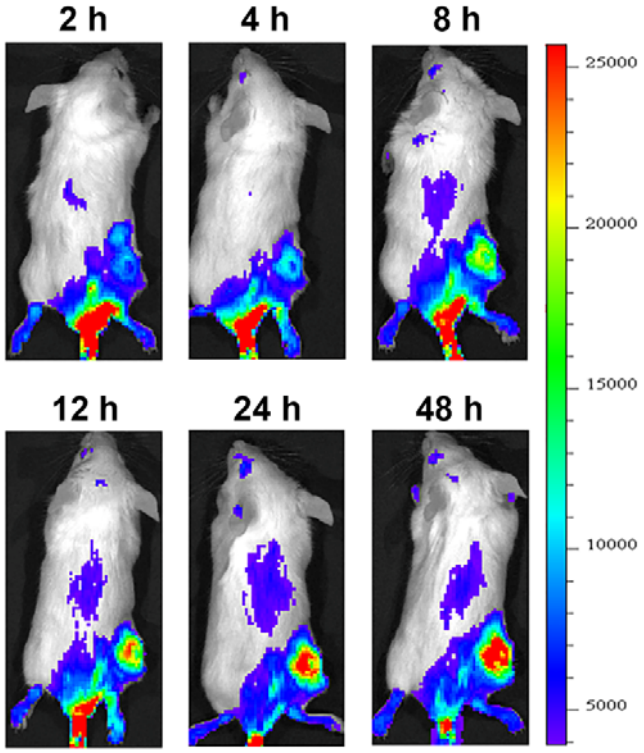

Fig. S19 *In vivo* NIRF imaging of 4T1-bearing Balb/c mice injected with BAP-based fluorescence probe.

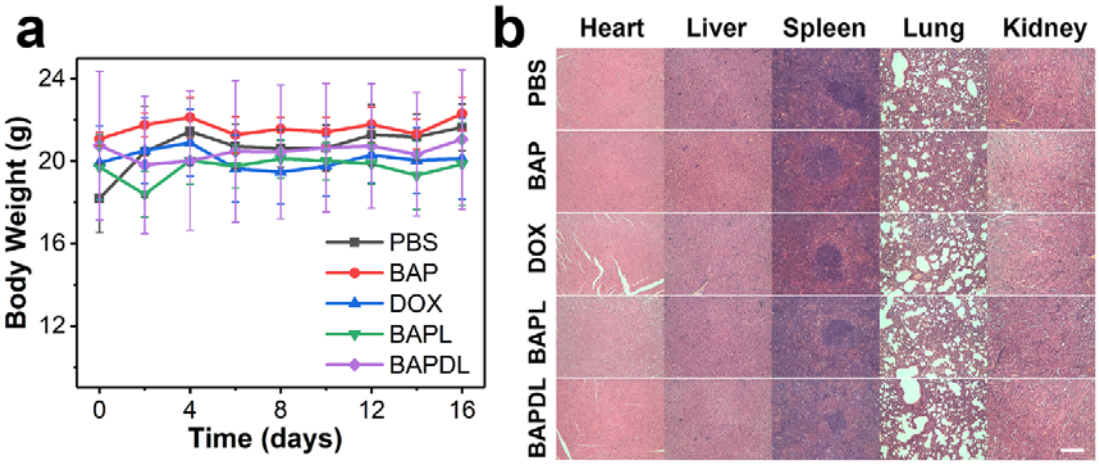

Fig. S20 a) Mean body weight changes in mice after treatment. b) Micrographs of H&E-stained major organs obtained from different groups (Scale bar: 100 μm).

References

1. L. Zhang, Y. Chen, Z. Li, L. Li, P. Saint-Cricq, C. Li, J. Lin, C. Wang, Z. Su and J. I. Zink, *Angew. Chem. Int. Ed.*, 2016, **55**, 2118.

2. Z. Sun, H. Xie, S. Tang, X. F. Yu, Z. Guo, J. Shao, H. Zhang, H. Huang, H. Wang and P. K. Chu, *Angew. Chem. Int. Ed.*, 2015, **54**, 11526.

3. G. J. Thomas, Jr., B. Prescott and D. E. Olins, *Science*, 1977, **197**, 385.

4. K. A. Willets, *Anal. Bioanal. Chem.*, 2009, **394**, 85.

5. J. Kneipp, H. Kneipp, M. McLaughlin, D. Brown and K. Kneipp, *Nano Lett.*, 2006, **6**, 2225.

6. J. J. Baraga, M. S. Feld and R. P. Rava, *Proc. Natl. Acad. Sci. U S A*, 1992, **89**, 3473.

7. N. T. Yu, C. S. Liu and D. C. O'Shea, *J Mol. Biol.,* 1972, **70**, 117.

8. A. Huefner, W. L. Kuan, K. H. Muller, J. N. Skepper, R. A. Barker and S. Mahajan, *ACS Nano*, 2016, **10**, 307.

9. W. Xie, L. Wang, Y. Zhang, L. Su, A. Shen, J. Tan and J. Hu, *Bioconjugate Chem.,* 2009, **20**, 768.